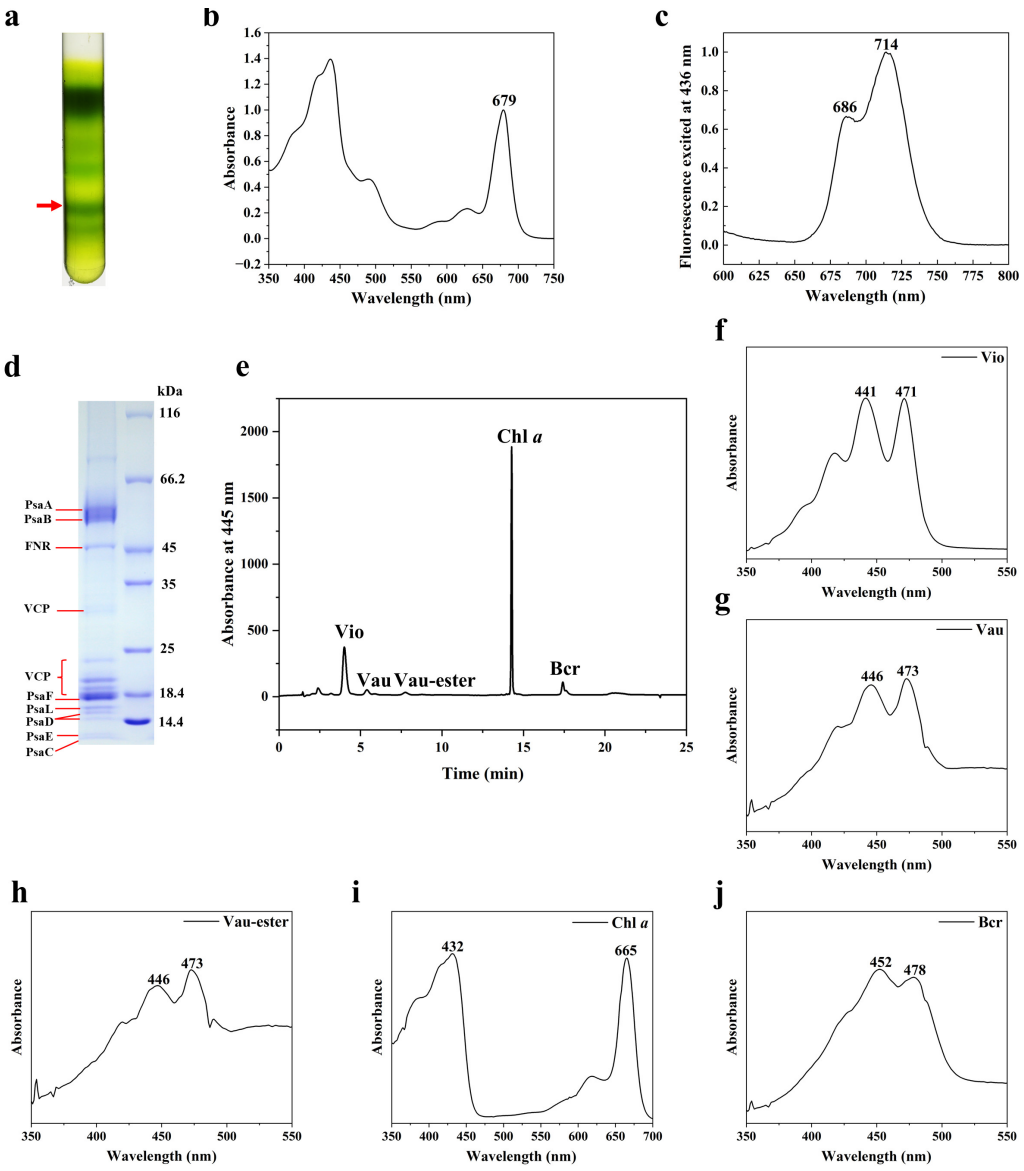

Extended Data Fig. 1 | Purification and Characterization of the PSI-VCP-FNR supercomplex from *Nannochloropsis oceanica*.

a, Sucrose density gradient centrifugation of solubilized *N. oceanica* thylakoid membranes. The band corresponding to the NoPSI-VCP-FNR supercomplex is indicated by a red arrow. **b,** Room-temperature absorption spectrum of the purified NoPSI-VCP-FNR sample. **c,** 77 K steady-state fluorescence emission spectrum of the NoPSI-VCP-FNR sample, excited at 436 nm. **d,** SDS-PAGE analysis of the NoPSI-VCP-FNR supercomplex. **e,** HPLC analysis of the pigment composition of the NoPSI-VCP-FNR sample, monitored at 445 nm. The major pigment peaks were identified as violaxanthin (Vio), vaucheriaxanthin (Vau), vaucheriaxanthin-ester (Vau-ester), chlorophyll *a* (Chl *a*), and β-carotene (Bcr) based on the characteristic absorption spectra of each fraction. **f-j,** Absorption spectra corresponding to the five major peaks labeled in panel **e**. Data are representative of at least three independent experiments.

a

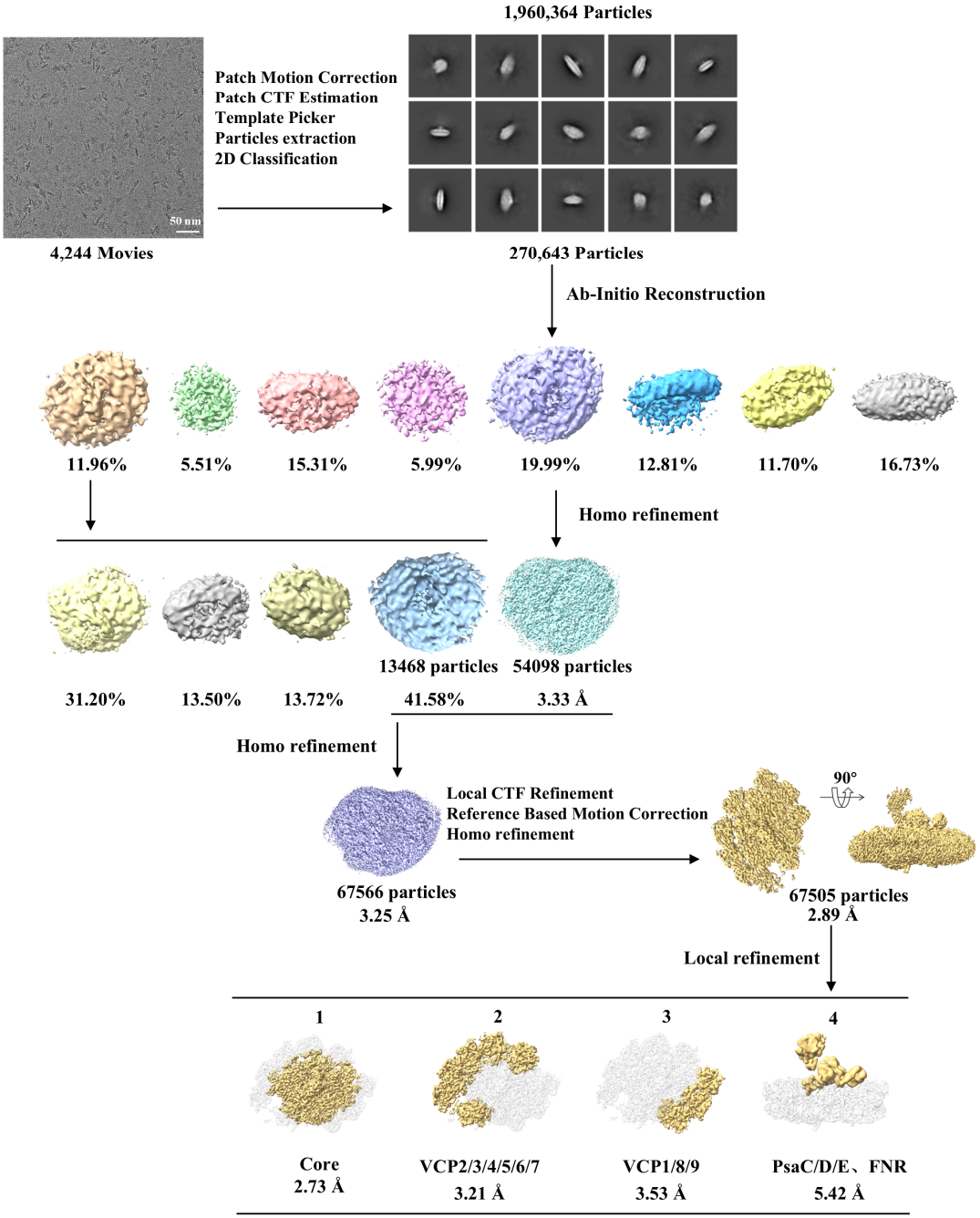
1,960,364 Particles
Patch Motion Correction
Patch CTF Estimation
Template Picker
Particles extraction
2D Classification
50 nm
4,244 Movies
270,643 Particles
Ab-Initio Reconstruction
11.96%
5.51%
15.31%
5.99%
19.99%
12.81%
11.70%
16.73%
Homo refinement
31.20%
13.50%
13.72%
13468 particles
41.58%
54098 particles
3.33 Å
Homo refinement
67566 particles
3.25 Å
Local CTF Refinement
Reference Based Motion Correction
Homo refinement
90°
67505 particles
2.89 Å
Local refinement
1
Core
2.73 Å
2
VCP2/3/4/5/6/7
3.21 Å
3
VCP1/8/9
3.53 Å
4
PsaC/D/E、FNR
5.42 Å

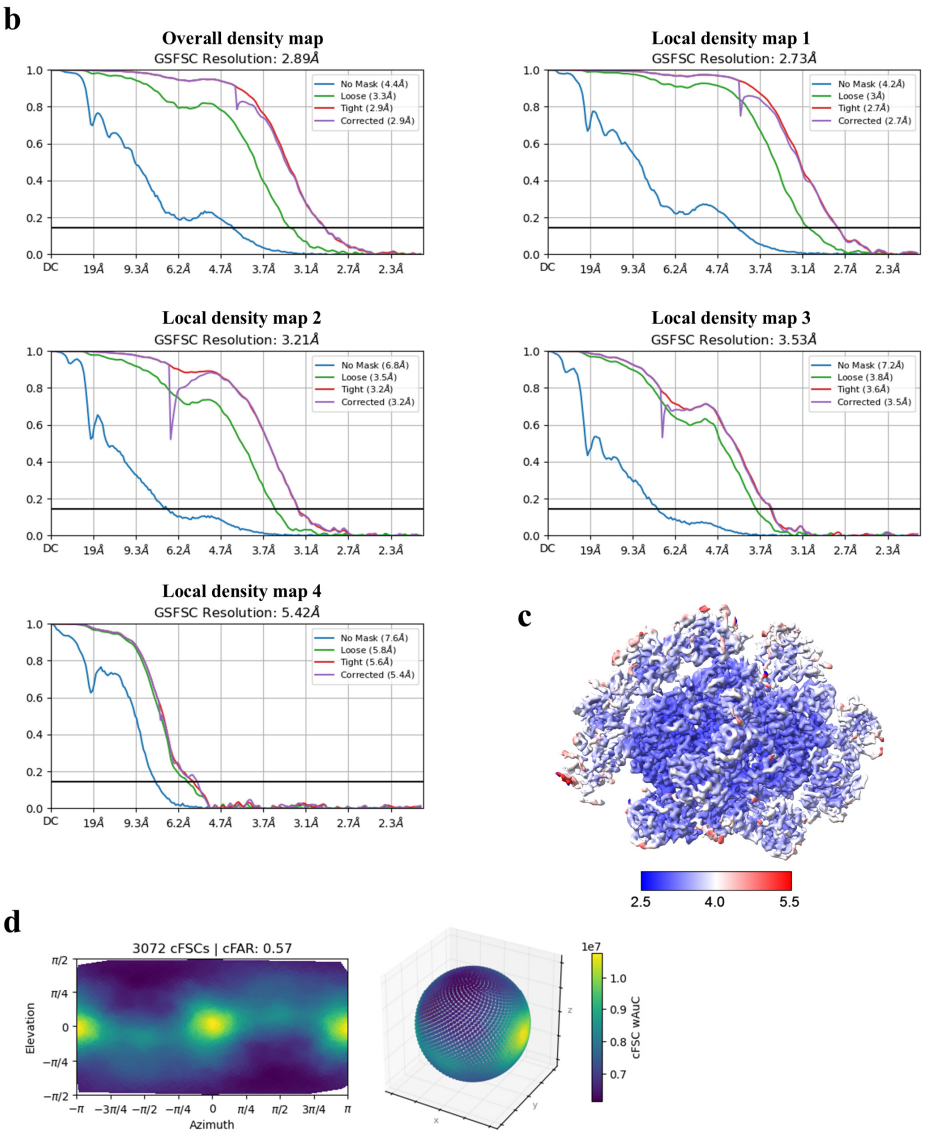

Extended Data Fig. 2 | Cryo-EM data processing and map validation of the NoPSI-VCP-FNR supercomplex.

a, Single-particle cryo-EM data processing workflow. **b,** Gold-standard Fourier shell correlation (FSC) curves for the overall and local density maps, using the 0.143 criterion. **c,** Local resolution distribution of the cryo-EM map, calculated in CryoSPARC. **d,** Angular distribution of particle orientations. A cFAR value above 0.5 indicates no significant preferred orientation.

a

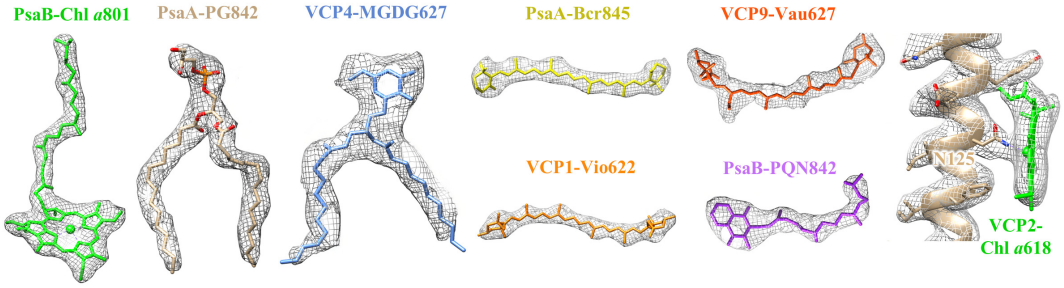
PsaB-Chl *a*801
PsaA-PG842
VCP4-MGDG627
PsaA-Bcr845
VCP9-Vau627
VCP1-Vio622
PsaB-PQN842
N125
VCP2-
Chl *a*618

b

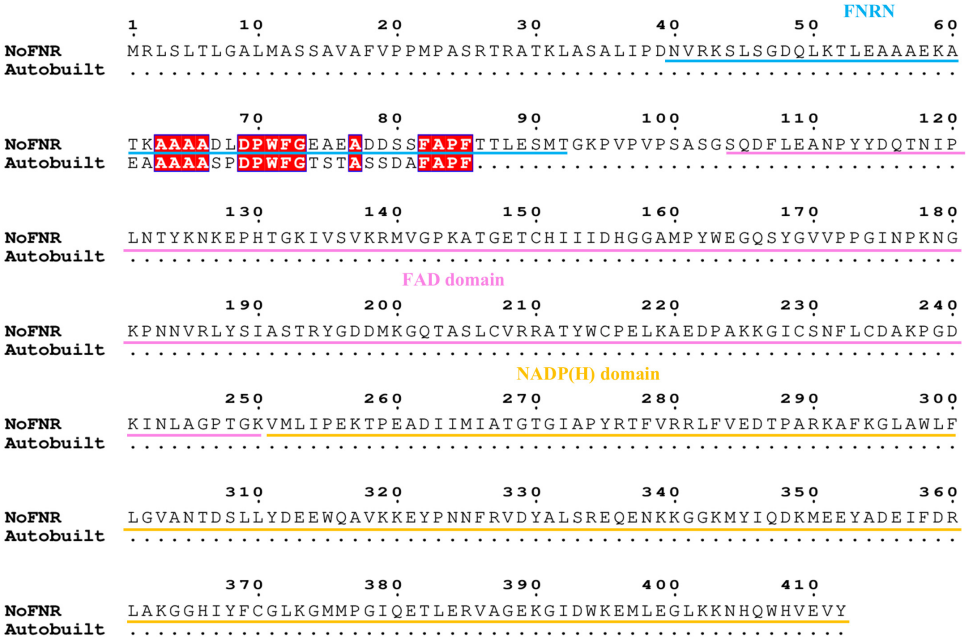
FNRN
NoFNR MRLSLTLGALMASSAVAFVPPMPASRTRATKLASALIPDNVRKSLSGDQLKTLEAAAEKA
Autobuilt
NoFNR TKAAAADLDPWFGEAEADDSSFAPFTTLESMTGKPVPVPSASGSQDFLEANPYYDQTNIP
Autobuilt EAAAAASPDPWFGTSTASSDAFAPF
NoFNR LNTYKNKEPHTGKIVSVKRMVGPKATGETCHIIIDHGGAMPYWEGQSYGVVPPGINPKNG
Autobuilt
FAD domain
NoFNR KPNNVRLYSIASTRYGDDMKGQTASLCVRRATYWCPELKAEDPAKKGICSNFLCDAKPGD
Autobuilt
NADP(H) domain
NoFNR KINLAGPTGKVMLIPEKTPEADIIMIATGTGIAPYRTFVRRLFVEDTPARKAFKGLAWLF
Autobuilt
NoFNR LGVANTDSLLYDEEWQAVKKEYPNNFRVDYALSREQENKKGGKMYIQDKMEEYADEIFDR
Autobuilt
NoFNR LAKGGHIYFCGLKGMMPGIQETLERVAGEKGIDWKEMLEGLKKNHQWHVEVY
Autobuilt

c

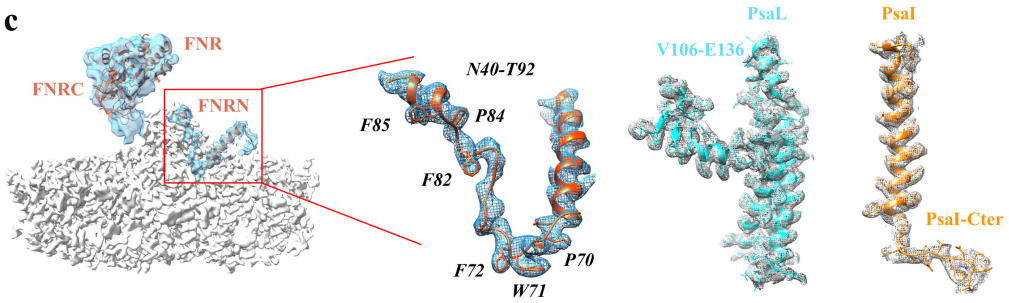
FNR
FNRC
FNRN
N40-T92
F85
P84
F82
F72
P70
W71
PsaL
V106-E136
PsaI
PsaI-Cter

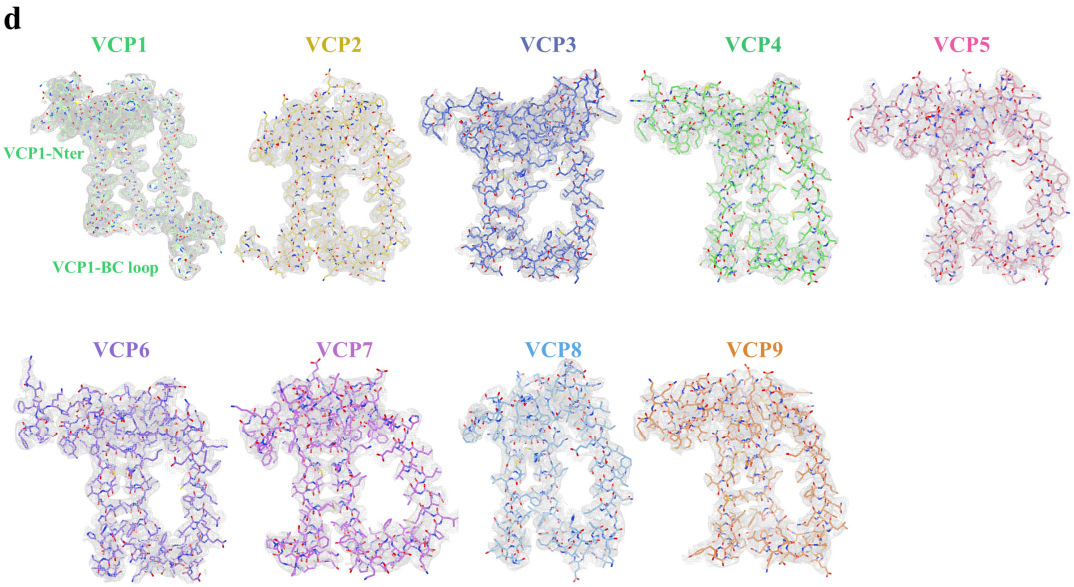

Extended Data Fig. 3 | Representative cryo-EM densities of ligands and VCP apoproteins, and identity of FNR. a, Representative cryo-EM densities for ligands in the supercomplex, including chlorophyll *a* (Chl *a*), β-carotene (Bcr), violaxanthin (Vio), vaucheriaxanthin (Vau), phosphatidylglycerol (PG), monogalactosyldiacylglycerol (MGDG), and phylloquinone (PQN). A separate view shows Chl *a*618 and its coordinating residue in VCP2. **b,** Sequence alignment between the *de novo* built model from ModelAngelo (Autobuilt) and the reference NoFNR sequence, with the FNRN, FAD- binding and NADP(H)-binding domains indicated by blue, pink and yellow lines, respectively. **c,** Cryo-EM density for FNR and its interacting subunits PsaL and PsaI. **d,** Cryo-EM density features for the apoprotein of each VCP subunit.

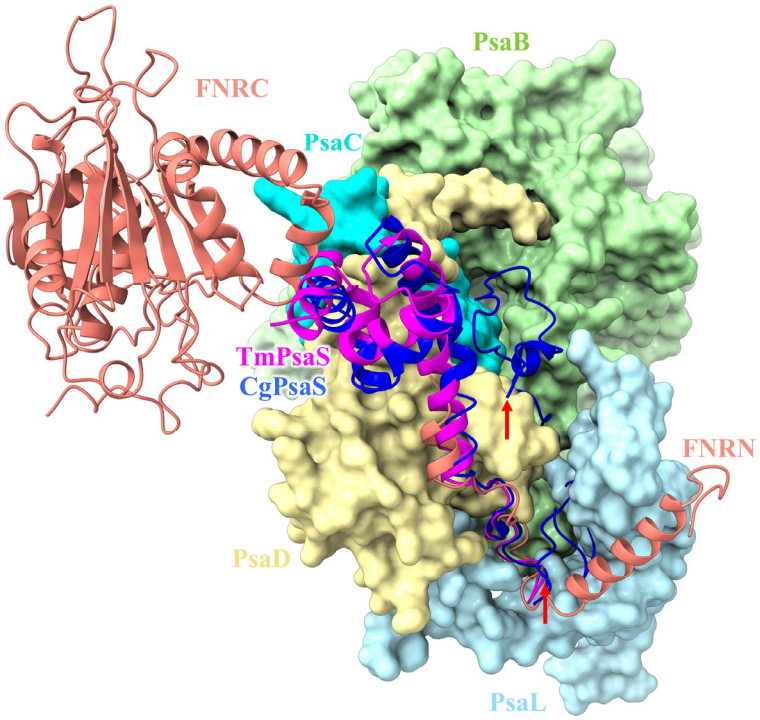

Extended Data Fig. 4 | Structural comparison of the NoFNR and PsaS from xanthophyte and diatom.

The PsaS subunits from xanthophyte *T. minus* (Tm, PDB: 9M4F) and diatom *C. gracilis* (Cg, PDB: 6LY5) are shown in magenta and blue cartoons, respectively. The FNR from *N. oceanica* are depicted in salmon cartoon, while other subunits are shown as colored surface. The N-terminus of Tm/CgPsaS is indicated by red arrow.

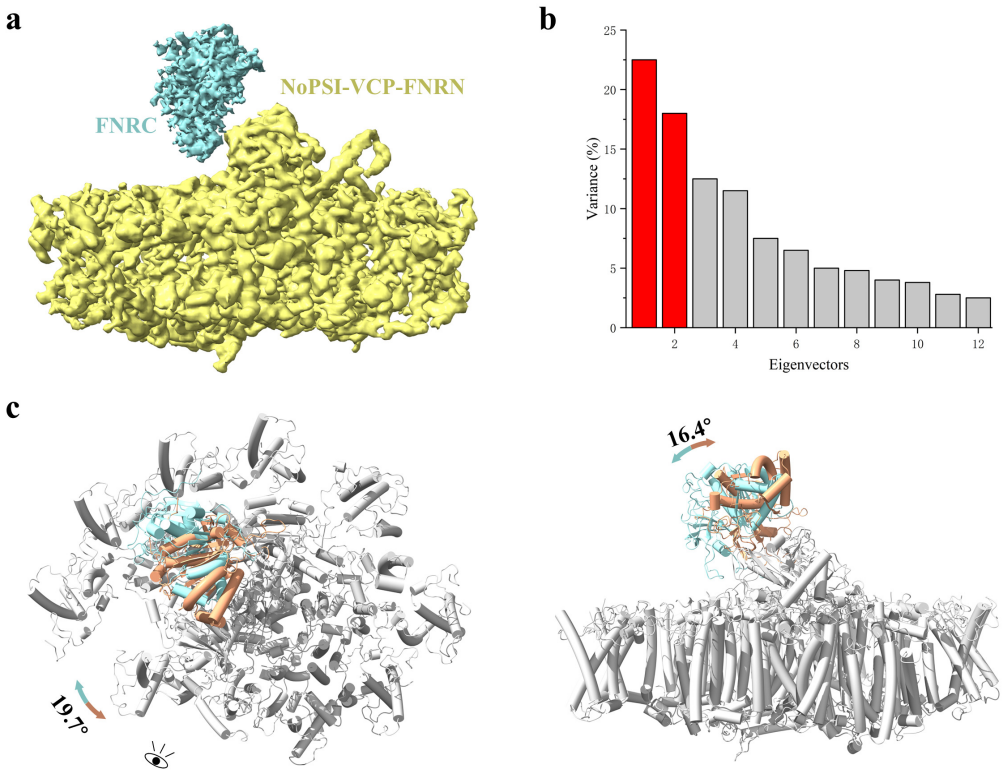

Extended Data Fig. 5 | Multibody refinement of the NoPSI-VCP-FNR supercomplex.

a, The two defined rigid bodies for refinement, corresponding to the NoPSI-VCP-FNRN moiety and the FNRC subunit, are colored yellow and cyan, respectively. **b,** Variance contributions of all 12 eigenvectors. **c,** Conformational flexibility of FNRC relative to the NoPSI-VCP-FNRN moiety along the second principal components (Eigenvectors #2). For the component, models were fitted into the Bin 1 and Bin 10 maps and superimposed on the NoPSI-VCP-FNRN moiety. Left and right panels show views from the stromal side and the membrane plane, respectively, with eye symbols indicating the viewing direction for the side views. The FNRC is shown in orange and cyan for the two states (Bins 1 and 10, respectively), and the NoPSI-VCP-FNRN moiety is shown in gray.

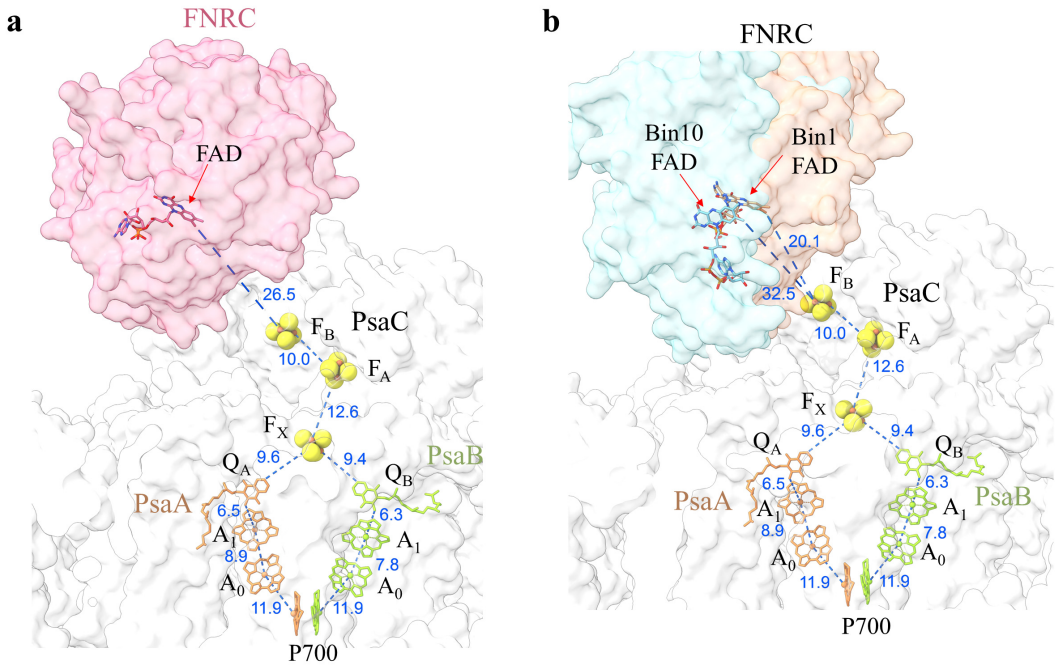

Extended Data Fig. 6 | Variation of inter-cofactor distances in the electron transfer chain.

a, Inter-cofactor distances in the electron transfer chain. FNRC is shown as pink surface, and other subunits are in white. **b**, Structural models fitted into the Bin 1 (FNRC in orange) and Bin 10 (FNRC in cyan) maps from the second principal component (Eigenvector #2) of the multi-body refinement. In (**a**) and (**b**), key electron carriers are depicted as sticks or spheres, including the P700 chlorophyll pair, chlorophylls at the A_0 and A_1 sites, phylloquinones (Q_A, Q_B), iron-sulfur clusters (F_X, F_A, F_B), and the FAD cofactor of FNR. Distances (Å) between adjacent cofactors are labeled.

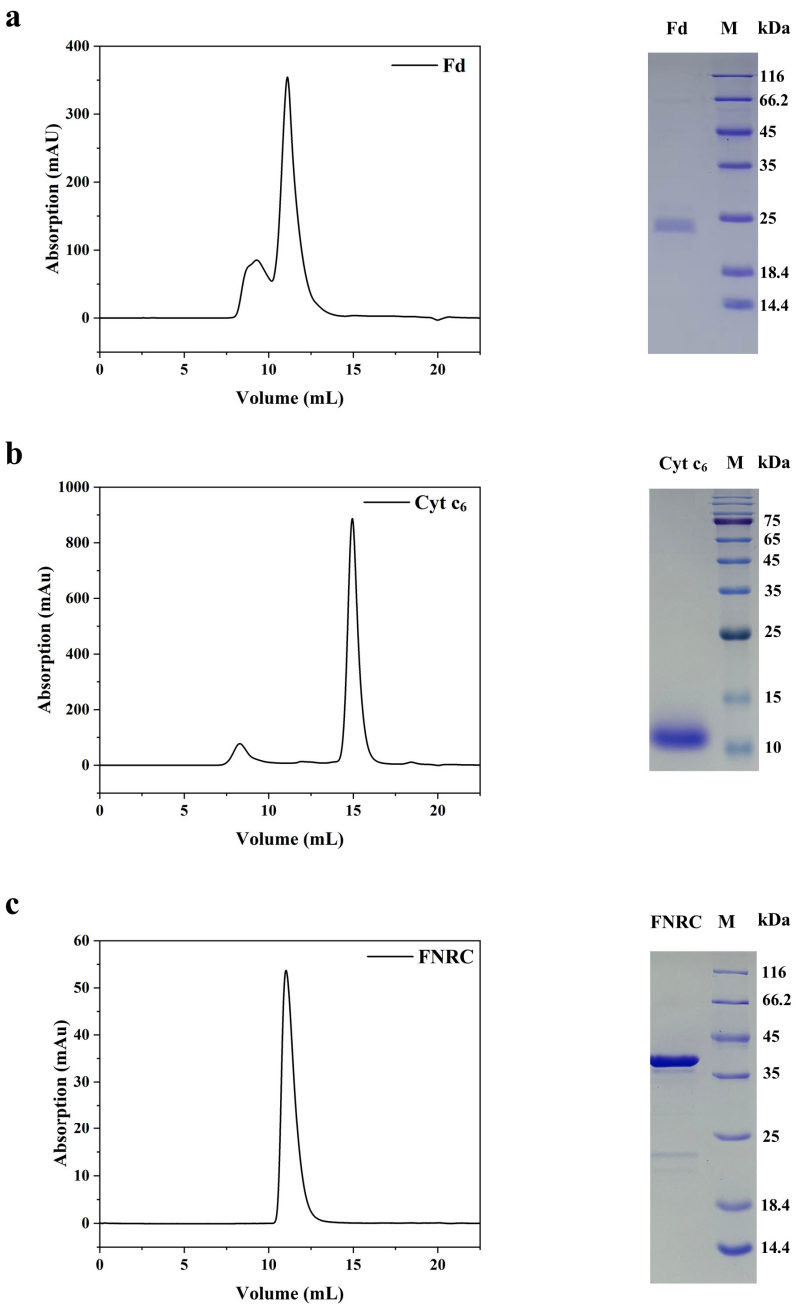

Extended Data Fig. 7 | Purification of recombinant electron carrier proteins from *N. oceanica*.

a-c, Purification of recombinant Fd (**a**), cytochrome c_6 (Cyt c_6) (**b**) and FNRC (**c**) from *N. oceanica* via a Superdex 75 Increase column, with purity confirmed by SDS–PAGE.

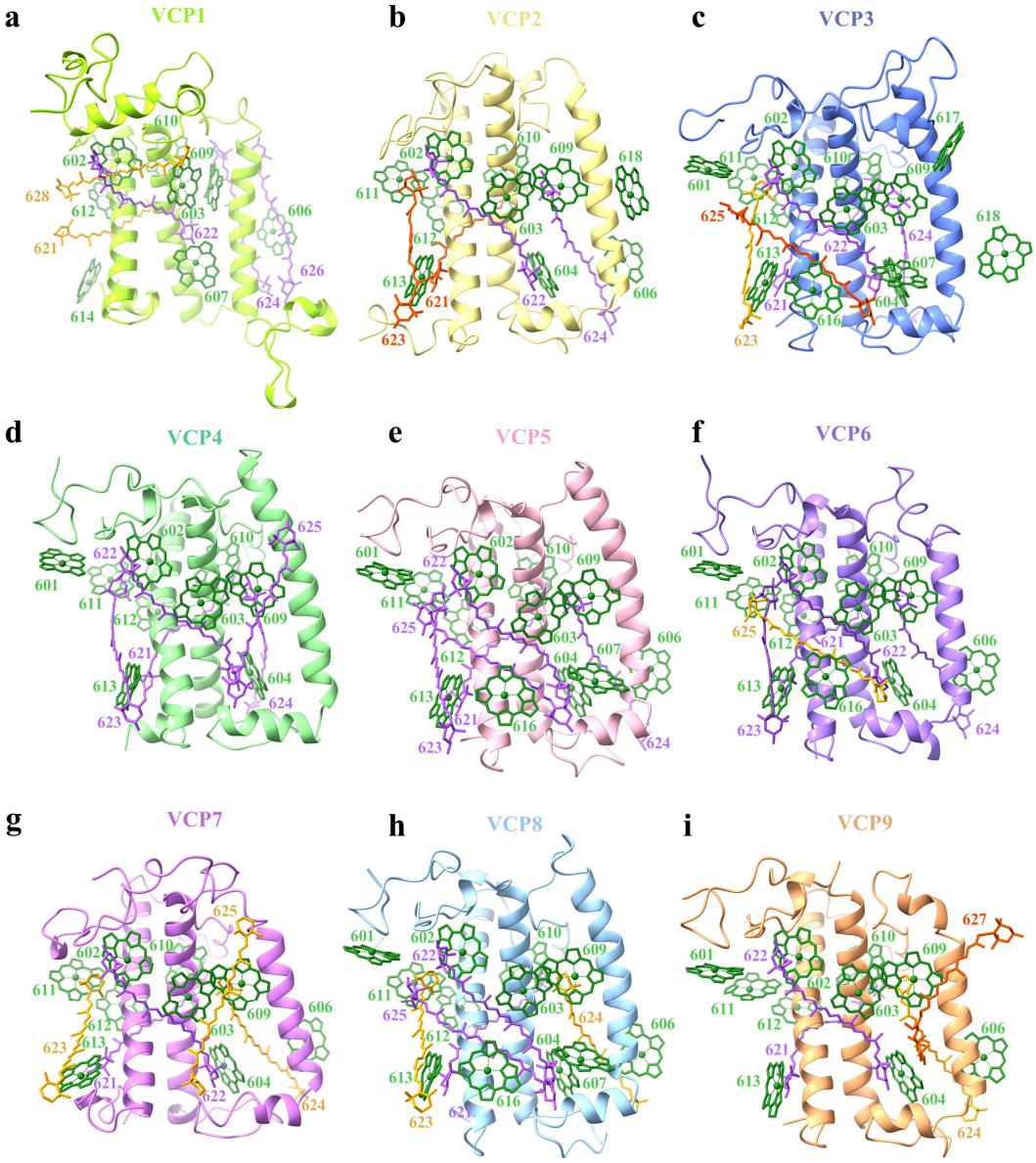

Extended Data Fig. 8 | Structure and pigment arrangement of the VCPs.
a–i, Structure and pigment distribution of VCPs1–9. The pigments chlorophyll *a* (Chl *a*), β-carotene (Bcr), violaxanthin (Vio), and vaucheriaxanthin (Vau) are shown as sticks and colored green, orange, purple, and orange-red, respectively. For clarity, the phytol tails of Chl *a* are omitted. All pigment molecules are labeled.

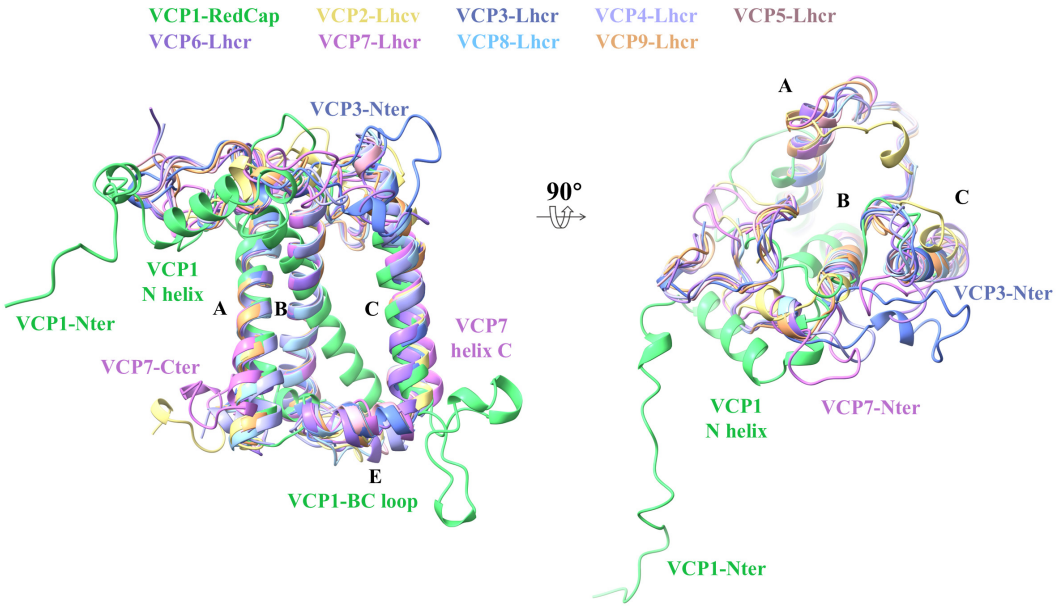

Extended Data Fig. 9 | Structure comparison of VCP apoproteins.
Structural superposition of the apoproteins of nine VCPs, shown in different colors. Unique structural features are labeled, including the N-terminal (Nter), C-terminal (Cter) regions and N-terminal helix (N helix).

Extended Data Table 1 | Cryo-EM data collection, refinement, and validation statistics

NoPSI-VCP-FNR (EMDB: 68619, PDB: 22RG)	
Data collection and processing	
Magnification	130,000
Voltage (kV)	300
Electron exposure (e^{-}/Å^2)	50
Defocus range (μm)	-1.5~-2.2
Pixel size (Å)	1.06
Symmetry imposed	C1
Initial particles images	1,960,364
Number of final particles	67,505
Map resolution (Å)	2.89
FSC threshold	0.143
Refinement	
Initial model used (PDB code)	6LY5
Model resolution (Å)	3.04
FSC threshold	0.5
Map sharpening B factor (Å^2)	-53.02
Model composition	
Non-hydrogen atoms	47278
Protein residues	4,207
Ligands	283
B factors (Å^2)	
Protein	119.81
Ligand	102.49
Root mean square deviations	
Bond lengths (Å)	0.004
Bond angles (°)	1.228
Validation	
MolProbity score	1.44
Clash score	4.55
Poor rotamers (%)	0.62
Ramachandran plot	
Favored (%)	96.66
Allowed (%)	3.29
Disallowed (%)	0.05